ACS APPLIED MATERIALS & INTERFACES

Research Article

www.acsami.org

Cross-Linking the Surface of Cured Polydimethylsiloxane via Hyperthemal Hydrogen Projectile Bombardment

Chao Bao,[†,⊗] Ke-Qin Xu,[†,⊗] Chang-Yu Tang,[†] Woon-ming Lau,[†] Cong-Bin Yin,[‡] Yan Zhu,[§] Jun Mei,[†] Jonathan Lee,[†] David Hui,[∥] Heng-Yong Nie,[*,⊥,#] and Yu Liu[*,†]

[†]Chengdu Green Energy and Green Manufacturing Technology R&D Center, Chengdu, Sichuan 610207, China

[‡]CCDC Downhole Service Company, CNPC, Chengdu, Sichuan 610051, China

[§]Faculty of Materials Science and Engineering, Kunming University of Science and Technology, Kunming 650093, China

[∥]Department of Mechanical Engineering, University of New Orleans, New Orleans, Louisiana 70148, United States

[⊥]Surface Science Western, The University of Western Ontario, 999 Collip Circle, London, Ontario N6G 0J3, Canada

[#]Department of Physics and Astronomy, The University of Western Ontario, London, Ontario N6A 3K7, Canada

ABSTRACT: Cross-linking of polydimethylsiloxane (PDMS) is increasingly important with recent focus on its top surface stiffness. In this paper, we demonstrate that hyperthermal hydrogen projectile bombardment, a surface sensitive cross-linking technology, is superior in enhancing the mechanical properties of a cured PDMS surface without significantly degrading its hydrophobicity. Both water contact angle measurements and time-of-flight secondary ion mass spectrometry are used to investigate the variations in surface chemistry and structure upon cross-linking. Using nanoindentation and atomic force microscopy, we confirm that the thickness of the cross-linked PDMS is controllable by the bombardment time, which opens opportunities for tuning cross-linking degree in compliance with arising requirements from the practice.

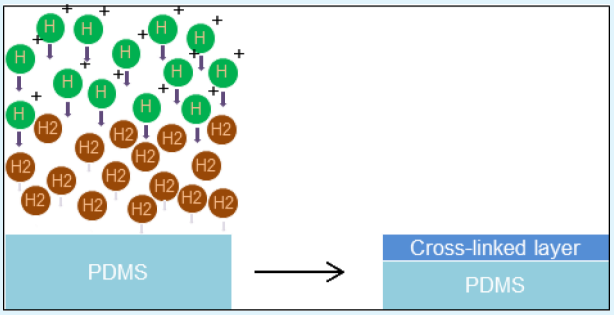

KEYWORDS: *hyperthemal hydrogen projectile bombardment, cross-linking, polydimethylsiloxane (PDMS), surface chemistry and mechanical properties, thickness of cross-linked PDMS*

1. INTRODUCTION

Polydimethylsiloxane (PDMS) has been widely used in various areas due to its low cost, high flexibility, controllable mechanical properties, and brilliant biocompatibility.[1−12] The physical and chemical properties of PDMS play important roles during its extensive applications in sensors and actuators.[13,14] Most work on PDMS has been focusing on tuning its surface properties. When used as a biomedical substrate, PDMS surfaces may affect cell attachment, spreading and differentiation.[1] Kurpinski et al.[5] noticed that the differentiation and proliferation of mesenchymal stem cells are related to the mechanical strain of a PDMS substrate. Eroshenko et al.[7] reported that the initial attachment and spreading of human embryonic stem cells (hESC) cells is sensitive to the stiffness of the PDMS substrate. Valamehr et al.[4] found that a native hydrophobic PDMS is efficient for the formation of embrydoid body (EB). Furthermore, in the soft stamping technology, a mechanically weak PDMS stamp would cause pattern roof collapse and lateral feature loss, which impact the resolution of the final products to over 100 nm.[12,15−17]

To render appropriate surface chemical and physical properties of PDMS for its specific applications, various treatments are applied to the material such as varying the cross-linker ratio, irradiating with plasma, UV/ozone treatment and the use of metal catalyzed reactions.[16] Eroshenko et al.[7] characterized PDMS substrates having different stiffness and directed the final cell types by varying the base to cross-linking agent ratio. Wang et al.[2] pointed out that the PDMS substrate with mechanical properties similar to living tissues can be obtained by varying the degree of cross-linking of the polymer network. Brown et al.[3] further used PDMS to examine the relationship between the material properties and cellular responses as a funcion of substrate stiffness by changing the concentration of the cross-linker. It has been reported that a silica-like layer can form by the oxygen plasma irradiation of the PDMS surface.[18,19] The modulus of the substrate increased after a short-time oxygen plasma treatment, while the surface energy increased, leading to a hydrophilic surface. UV or UV/ozone radiation is a less abrasive approach compared to oxygen plasma, but still allows for the formation of a silica-like layer.[20−24] Other surface modification approaches, such as hydrosilylation treatment,[25] peroxide[26−29] or metal catalyzed reactions,[30] have also been widely used to change the surface

Received: January 7, 2015
Accepted: April 7, 2015
Published: April 7, 2015

DOI: 10.1021/acsami.5b00190
ACS Appl. Mater. Interfaces 2015, 7, 8515−8524

energy or form a hybrid membrane as an insulation barrier on a PDMS substrate.

Recently, a surface sensitive cross-linking technology, namely, hyperthermal hydrogen induced cross-linking (HHIC), has been developed as a novel surface modification method that selectively cleaves C−H bonds.[31−36] The carbon radicals created by the hyperthermal hydrogen projectile bombardment results in cross-linking of the hydrocarbons on the top surface. In this paper, we present an application of HHIC treatment in creating a cross-linked layer on the PDMS surface and its characterizations using various techniques to probe the surface chemistry, mechanical properties and the thickness of the cross-linked layer. Water contact angle measurement[37] is a simple but powerful approach to evaluate the surface hydrophobicity of the HHIC-treated PDMS. X-ray photoelectron spectroscopy (XPS) probes chemical states of elements[38] in the top several nanometers, thus sensitive in assessing chemical changes on the surface of the PDMS[39,40] samples upon their HHIC treatment. Though less surface sensitive in comparison with XPS, attenuated-total-reflection Fourier transform infrared (ATR-FTIR) spectroscopy probes the functional groups of PDMS within 1 μm or so.[40−42] Time-of-flight secondary ion mass spectrometry (TOF-SIMS)[43] is a surface sensitive technique probing surface chemistry and structure[44,45] of the PDMS upon the HHIC treatment by measuring secondary ion fragments generated from the surface as resulted from the bombardment of the primary ion beam. Atomic force microscopy (AFM) not only images the surface morphology but also probes mechanical properties via phase shift imaging.[46,47] The mechanical properties of the HHIC-treated PDMS substrates are also examined using a nano-indenter.[48] With those characterization techniques, we provide a thorough understanding of the cross-linked layer by the HHIC technology on the surface of a cured PDMS substrate.

2. EXPERIMENTAL SECTION

2.1. Materials and Preparation of PDMS Substrates. Sylgard 184 silicone elastomer kit was purchased from Dow Corning (Midland, MI). The silicone elastomer base and curing agent were mixed with a volume ratio of 10:1 in a beaker. A homogeneous mixture was obtained by continuous manual stirring with a glass rod for 5 min in a beaker. In order to remove the bubbles from the mixer to avoid the influence on the homogeneity and mechanical properties of PDMS, the mixture was placed into a vacuum drier for 20 min. After degassing, the mixture was poured into a tensile test mold with five chambers of 2 mm depth. Final, these PDMS substrates were cured in an oven at 110 °C for 40, 60, 90 and 180 min. Unless mentioned otherwise, most of the analyses were carried on PDMS samples cured for 180 min.

2.2. Hyperthermal Hydrogen Induced Cross-Linking. A cross-linking treatment of PDMS was carried out by a home-built HHIC system. The pressure inside this reactor was pumped down to 6×10^{-4} Pa after samples were placed into the reactor. Then hydrogen gas was introduced into the electron-cyclotron-resonance (ECR) microwave plasma chamber at a flow rate of 14 SCCM to reach a final pressure of 0.1 Pa. The microwave plasma power in the ECR was set to 300 W. Protons generated in the ECR were extracted from the plasma and accelerated into the drift zone by two aperture plates with a negative potential difference of −10 V. In the drift zone, energy of hydrogen molecules was increased up to ∼10 eV[36,49−52] after a series of collisions with the accelerated protons through a chain reaction of the energetic protons and hydrogen projectiles. Residual electrons and protons were prevented successively by two different electric fields facilitated above the sample with a voltage of −50 V and +100 V, respectively. Finally, only neutral hyperthermal hydrogen projectiles bombarded on the sample surface to cross-link the molecules on and near the surface. The degree of cross-linking was controlled by varying bombardment time in this study.

2.3. Characterizations and Methods. *Contact Angle Measurement.* Measurements of water contact angle were carried out using a contact angle goniometer (Kruss DSA25). A deionized water droplet with a volume of 5 μL was used for all measurements. At least five locations on each sample were probed and averaged for the reported results.

XPS. The XPS analyses were carried out with a Kratos Axis Ultra spectrometer using a monochromatic Al Kα source (15 mA, 14 kV). The instrument work function was calibrated to give an Au $4f_{7/2}$ metallic gold binding energy (BE) of 83.95 eV and the spectrometer dispersion was adjusted to give a binding energy of 932.63 eV for metallic Cu $2p_{3/2}$. The Kratos charge neutralizer system was used on all specimens. Survey and high-resolution spectra were collected (on an area of 300 × 700 μm) with a pass energy of 160 and 20 eV, respectively. CASAXPS processing software v.2.3.16 was used to analyze the XPS spectra.

TOF-SIMS. An ION-TOF (GmbH) TOF-SIMS IV equipped with a bismuth cluster liquid metal ion source was used. A 25 keV Bi_3^+ primary ion beam pulsed at 10 kHz was used to bombard the sample surface to generate secondary ions. The positive or negative secondary ions were extracted from the sample surface, mass separated and detected via a reflectron-type of time-of-flight analyzer, allowing parallel detection of ion fragments having a mass/charge (m/z) ratio up to ∼900 within each cycle (100 μs). A pulsed, low energy electron flood was used to neutralize sample charging. Negative and positive ion mass spectra were collected at 128 × 128 pixels over an area of 350 × 350 μm at three spots. The base pressure of the analytical chamber is 1×10^{-8} mbar. The 180 min-cured PDMS subjected to HHIC treatment for 30 and 600 s and the control were examined using TOF-SIMS. Spectra in both polarities were calibrated using the H and C ion species. Mass resolutions of PDMS characteristic species Si^+, $C_3H_5^+$, C_4H^- and $Si_2C_3H_9O_3^-$ were 3500, 5000, 4800 and 5400, respectively.

Nanoindentation. The hardness and reduced modulus of the cross-linked layer of PDMS substrates were measured using a nanoindenter (Hysitron TI 950 TriboIndenter), which has a high force sensitivity (<30 nN) and high displacement sensitivity (<0.2 nm). Surface forces exerted on the probe were measured while the probe was indented into the surface, from which the mechanical properties of the cross-linked film on PDMS were extracted.

Atomic Force Microscopy. The surface morphology and phase shift angles of the cross-sectioned PDMS substrate (180 min-cured) subjected to HHIC treatment for 600 s and the control were studied with dynamic force mode and phase shift image of an AFM (Park Systems XE-100) . Used in this experiment was a cantilever having a spring constant of 40 N/m, a resonant frequency of 300 kHz and a tip radius of 10 nm. In this mode, the cantilever is vibrated around its resonance frequency and its reduced amplitude is used as the feedback parameter for imaging. Under this feedback condition, a phase shift of the cantilever is a measure of mechanical properties of the sample surface, useful in differentiating components having different mechanical properties. The cross sections were made by cutting using a razor blade. The cantilever was placed above the edge of the cross section to search for the very edge, followed by imaging the edge in an area of 1 × 1 μm with a pixel density of 256 × 256. The images were obtained with a scan rate of 1.5 Hz in air.

FTIR. ATR-FTIR spectra were obtained using a Thermo Scientific Nicolet iS10 FT-IR spectrometer, equipped with an ATR accessory. The internal crystal element used for the ATR configuration was ZnSe. The incident angle of the IR irradiation was 42°. The experiment was conducted on a 180 min cured PDMS and HHIC-treated PDMS samples for various durations. ATR-FTIR spectra were collected at a 0.48 cm^{-1} resolution for 32 scans over three areas (1.5 mm in diameter) on each sample. The spectra over the three spots were baseline corrected and averaged

DOI: 10.1021/acsami.5b00190
ACS Appl. Mater. Interfaces 2015, 7, 8515−8524

3. RESULTS AND DISCUSSION

3.1. Surface Wettability of the PDMS Surface. Water contact angles were used to assess the wettability of the cross-linked PDMS surface. Shown in Table 1 are the data obtained for PDMS substrates (cured for different times) subjected to HHIC treatment for 600 s. The contact angles for as-cured PDMS samples before HHIC treatment were 116°−120°. It is thus clear that the curing time had only a minimal impact on CAs. According to Dow Corning's technical information on the Sylgard 184 elastomer kit, curing time at 100 °C is 35 min, so the 40 min curing time at 110 °C in our case is long enough to cure Sylgard 184, which is why there were no much changes in CAs observed among PDMS samples cured with a time longer than 40 min (i.e., 60, 90 and 180 min).

Table 1. CA (deg) Data for PDMS Samples (Cured for Different Times) Subjected to HHIC Treatment for 600 s

curing time (min)	control	HHIC-treated	decrement
40	120 ± 0	101 ± 2	19
60	117 ± 1	99 ± 1	18
90	116 ± 2	100 ± 3	16
180	117 ± 2	96 ± 2	21

Upon the 600 s HHIC treatment, the reduction in CAs were only 16−21° so that the CAs were still more than 90° (96°−101°). In other words, the HHIC-treated PDMS, even at an extended treatment time of 600 s, was still hydrophobic. Other surface treatment methods, such as UV/Ozone and oxygen plasma, rendered CAs <10°, a reduction of more than 90° in comparison with the pristine samples.[53−56] This is because these conventional surface modification methods resulted in surface oxidation of the methyl groups in PDMS. From the CAs measured before and after the HHIC treatment, we can thus infer that our HHIC treatment has a minimal impact on the surface chemistry of the PDMS.

Shown in Figure 1 are CAs for the 40 and 180 min cured PDMS substrates as a function of HHIC treatment time. There are no significant differences in CAs between the two samples when subjected to the same HHIC treatment time. It is thus clear that the HHIC treatment only slightly degraded the hydrophobicity of the PDMS surfaces and the surface remained hydrophobic. By contrast, cross-linked PDMS using high energy irradiation such as oxygen plasma led to a hydrophilic surface as the surface was oxidized.[53−56] It is clear that HHIC technology is superior in cross-linking PDMS while keeping the surface chemistry largely intact in comparison with the conventional methods such as plasma, UV or UV/ozone radiation.

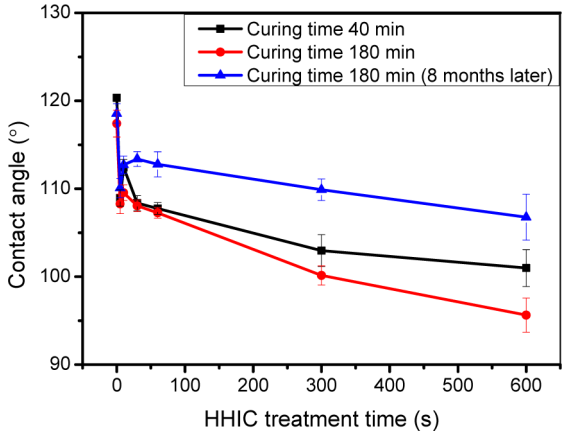

Figure 1. CAs measured on the 40 and 180 min cured PDMS substrates as a function of HHIC treatment time. Also shown are the CAs measured for the HHIC-treated, 180 min cured PDMS samples after 8 months.

We also checked the CAs on the 180 min cured PDMS samples after 8 months, which are also plotted in Figure 1. It is found that CAs of the HHIC-treated PDMS samples recovered to some extent, but still less than the control. This may be explained by adsorption of hydrocarbons on the HHIC-treated PDMS samples. Alternatively, migration of lower mass silicone moieties in the PDMS elastomer to the surface may take place,[39] which will result in a similar trend of increased CAs. In fact, even for the UV/ozone and plasma-treated PDMS surfaces, which were hydrophilic as characterized by CA values <10°, the CAs recovered eventually.[14,39]

3.2. Surface Chemistry of HHIC-Treated PDMS. To further understand the surface chemistry of the HHIC-treated PDMS samples, we carried out XPS analyses. The survey-scan XPS spectra obtained on a pristine, 180 min-treated PDMS (hereafter referred to as the control), the 30 s- and 600 s-treated PDMS samples are shown in Figure 2. The atomic percentages of carbon, oxygen and silicon determined from the spectra shown in Figure 2 for the three samples are listed in Table 2. It is clear that there are no significant changes in the compositions of the three constituent elements (i.e., carbon atomic composition 49−51%, oxygen 30−33% and silicon 18−21%) of PDMS (hydrogen is not detectable by XPS) before and after the HHIC treatment. In comparison, a dramatic

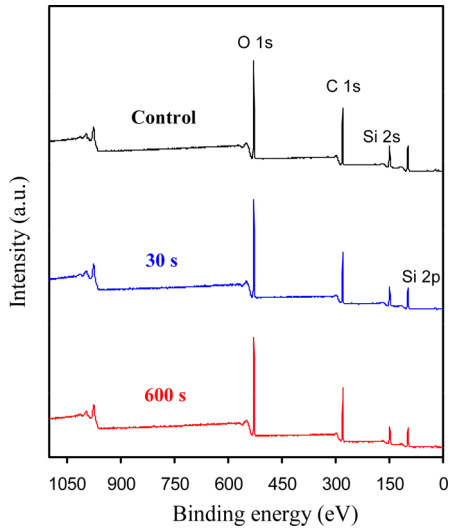

Figure 2. Survey-scan XPS spectra obtained on the control, the 30 s- and 600 s-treated PDMS samples.

Table 2. Atomic Percentages of Carbon, Oxygen and Silicon Determined from the XPS Survey-Scans Obtained on the Control, the 30 s- and 600 s-Treated PDMS Samples

samples	C 1s (%)	O 1s (%)	Si 2p (%)
control	49.1	30.0	20.9
30 s	48.9	32.5	18.6
600 s	50.7	31.3	18.0

DOI: 10.1021/acsami.5b00190
ACS Appl. Mater. Interfaces 2015, 7, 8515−8524

decrease in carbon atomic composition of PDMS to 23% upon a 13 min UV/ozone treatment and to 29% for a corona discharge treatment.[39,53] Therefore, our XPS results confirmed that there were no significant changes in surface chemistry of the PDMS samples. In order to see if there are any minimal chemical shifts in the three elements upon the HHIC treatment, we carried out high-resolution scans for the three elements.

The high-resolution C 1s peaks are shown in Figure 3. The chemical component analysis results of C 1s high-resolution

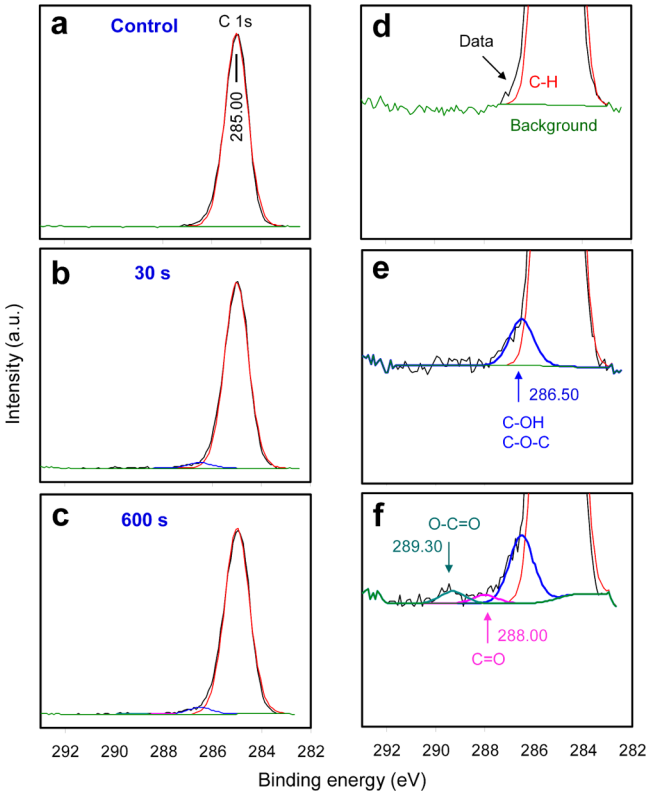

Figure 3. C 1s high-resolution XPS peaks for (a) the control, (b) the 30 s- and (c) 600 s-treated PDMS samples. The spectra in panels d–f are magnifications of those in panels a–c, respectively, which are used to show whether there are peaks of C—OH, C—O—C, C═O and O—C═O.

Table 3. Chemical Components as a Percentage of Total Carbon Determined from C 1s High-Resolution XPS Data

samples	C—C, C—H (%)	C—OH, C—O—C (%)	C═O (%)	O—C═O (%)
control	100			
30 s	97.1	2.9		
600 s	95.1	3.8	0.5	0.7

XPS data are summarized in Table 3. For the control, the C 1s peak shows that the C—H component explains 100% of the carbon peak. However, the C—H component reduced to 97.1% and 95.1% for the 30 s- and 600 s-treated PDMS samples, respectively. On the 30 s-treated PDMS sample, 2.9% of the carbon peak was found to be associated with C—OH and C—O—C components. When the HHIC treatment time increased to 600 s, these two components increased to 3.8% of the carbon peak. Moreover, the presence of C═O and O—C═O components explained 0.5% and 0.7% of the carbon peak, respectively. We infer that the observed oxidation of the hydrocarbon was perhaps due to reaction between oxygen (in air) and residual carbon radicals on the surface after the HHIC-treated PDMS samples were taken out from the reactor. The XPS results thus suggest that the degree of the oxidation on the surface is minimal even for the 600 s-treated PDMS sample. Nevertheless, this observation provides explanation to the decreased CAs observed on the HHIC-treated PDMS samples (Figure 1), that is, the reduced CAs are due to a slightly oxidized surface (resulting in an increased surface energy).

Shown in Figure 4 are high-resolution Si 2p and O 1s peaks. There are no significant changes detected in the Si 2p and O 1s

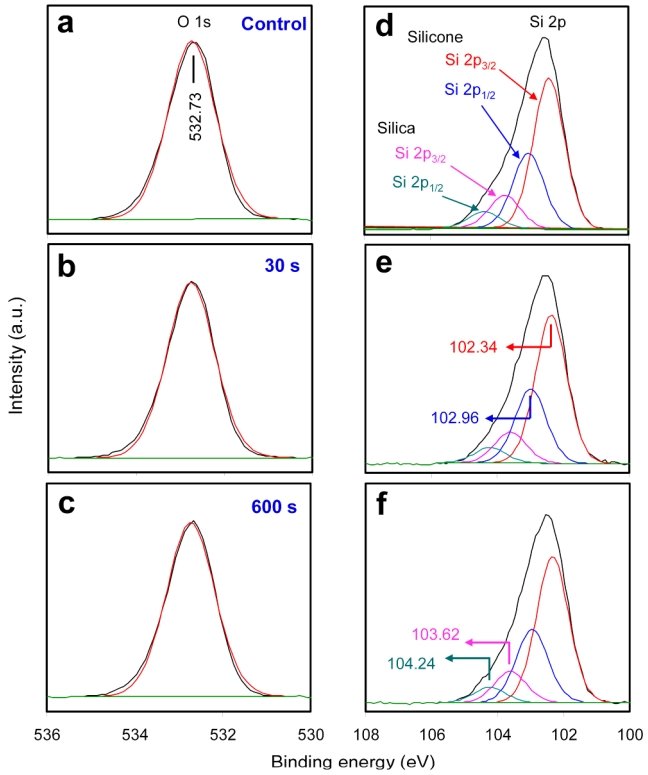

Figure 4. O 1s and Si 2p high-resolution XPS data for (a, d) the control, (b, e) the 30 s and (c, f) 600 s-treated PDMS sample, respectively.

peaks for the control, the 30 s- and 600 s-treated PDMS samples. The Si 2p peaks are convoluted by four components, namely, two spin–orbit doublets[57] of Si $2p_{3/2}$ and Si $2p_{1/2}$ for silicone and silica, respectively. The separation between the silicone and silica peaks is 1.33 eV. The silicone and silica compositions are approximately 82–83% and 17–18%, respectively for the three samples. Because silica composition is absent from a pure PDMS,[58] we infer that the silica detected in the PDMS samples originates from the Sylgard 184 system, which has also been discussed found before.[41,59]

3.3. Cross-Linked PDMS Assessed by TOF-SIMS. Shown in Figure 5 are positive and negative secondary ion mass spectra in m/z 25–225 for the control and the HHIC-treated PDMS for 30 and 600 s, in which the vast majority of silicone characteristic species are denoted in the figure. Abundant positive ion species shown in Figure 5a are Si^+ (m/z 28), $SiCH_3^+$ (43), $SiC_3H_9^+$ (73), $Si_2C_3H_{15}O^+$ (147), $Si_3C_3H_{15}O_3^+$

DOI: 10.1021/acsami.5b00190
ACS Appl. Mater. Interfaces 2015, 7, 8515–8524

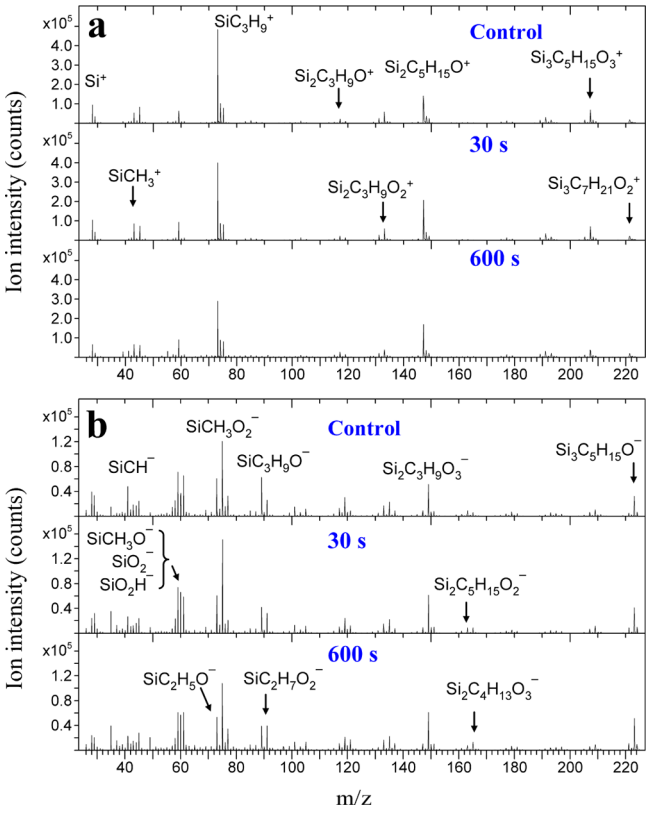

Figure 5. Positive (a) and negative (b) secondary ion mass spectra of the control and HHIC-treated PDMS samples for 30 and 600 s.

(207) and $Si_3C_7H_{21}O_2^+$ (221). Shown in Figure 5b are negative ion species characteristic to silicone, which are $SiCH^-$ (41), $SiCH_3O^-$ (59), SiO_2^- (60), SiO_2H^- (61), $SiC_2H_5O^-$ (73), $SiCH_3O_2^-$ (75), $SiC_3H_9O^-$ (89), $SiC_2H_7O_2^-$ (91), $Si_2C_3H_9O_3^-$ (149), $Si_2C_5H_{15}O_2^-$ (163), $Si_2C_4H_{13}O_3^-$ (165) and $Si_3C_5H_{15}O^-$ (223).

After analyses on these positive ion mass spectra, we conclude that there are no significant differences in the abundance of these species for the three samples. This experimental observation suggests that the positive ion species are uninformative in revealing differences caused by the HHIC treatment on the PDMS samples. By contrast, in the negative ion species, as clearly shown in Figure 6, we noticed that species at m/z 89 and 91, i.e., $SiC_3H_9O^-$ and $SiC_2H_7O_2^-$, vary oppositely as a function of HHIC treatment time, namely, the intensity of $SiC_3H_9O^-$ decreases while that of $SiC_2H_7O_2^-$ increases. This trend is also observed when comparing species at m/z 163 and 165, i.e., $Si_2C_5H_{15}O_2^-$ and $Si_2C_4H_{13}O_3^-$. To extract useful information from this experimental observation, we investigate as how these species are fragmented and whether they have connections useful in revealing the structural changes in HHIC-treated PDMS samples.

Figure 7 denotes ion fragmentation of $SiC_3H_9O^-$ and $Si_2C_5H_{15}O_2^-$ vs $SiC_2H_7O_2^-$ and $Si_2C_4H_{13}O_3^-$. The ion fragments $SiC_3H_9O^-$ and $Si_2C_5H_{15}O_2^-$ contain an end group of SiC_3H_9 at one end and an oxygen atom at the other. The unpaired oxygen species presents the negative charge. By contrast, $SiC_2H_7O_2^-$ and $Si_2C_4H_{13}O_3^-$ are terminated by an oxygen species at both ends, with one of them grabbing a proton to become neutralized and the other being unpaired to present the negative charge. The increase in intensities of $SiC_2H_7O_2^-$ and $Si_2C_4H_{13}O_3^-$ combined with the decrease in intensities of

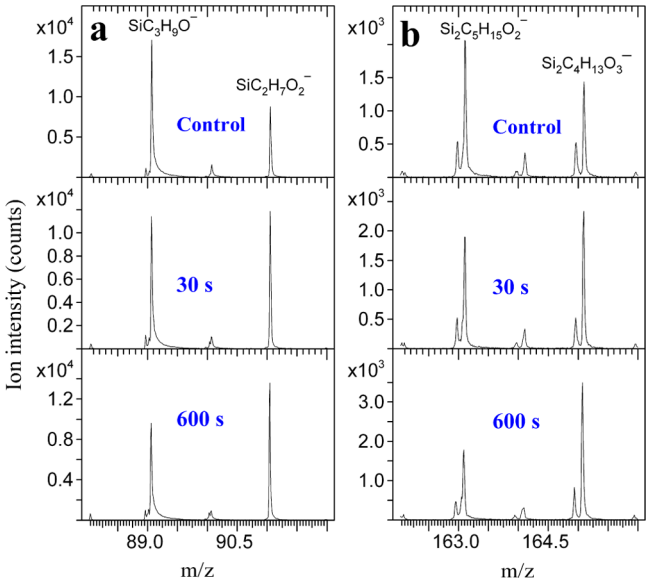

Figure 6. Negative secondary ion mass spectra of the control and HHIC-treated PDMS for 30 and 600 s in m/z ranges of (a) 88−92 (a) and (b) 162−165, showing the variations of the two species in each m/z range.

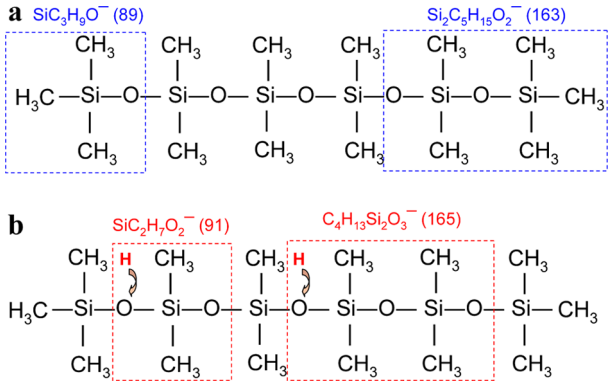

Figure 7. Ion species fragmented from silicone at (a) m/z 89 and 163 and (b) m/z 91 and 165.

$SiC_3H_9O^-$ and $Si_2C_5H_{15}O_2^-$ provide an analytical criterion in understanding how the presence of the end group (SiC_3H_9) affect the fragmentation of the PDMS samples.

With the two groups of negative ion species separated by an m/z difference of 2 identified as being useful in gauging the degree of cross-linked PDMS by the HHIC treatment, we compare in Figure 8 the intensity ratios between $SiC_3H_9O^-$ and $SiC_2H_7O_2^-$, as well as $Si_2C_5H_{15}O_2^-$ and $Si_2C_4H_{13}O_3^-$ as a function of HHIC treatment time. For the 180 min cured PDMS control, the two ratios are 2.23 ± 0.49 and 1.28 ± 0.35, respectively, meaning that the species containing the end-group ($SiC_3H_9O^-$ and $Si_2C_5H_{15}O_2^-$) are more abundant than those without the end-group ($SiC_2H_7O_2^-$ and $Si_2C_4H_{13}O_3^-$). Upon the 30 s HHIC treatment, the ratios decreased to around 1. When subjected to the 600 s HHIC treatment, the ratios become 0.86 ± 0.03 and 0.48 ± 0.02, respectively, indicating that species containing the end-group are now less abundant than those without the end-group. These two groups of ion species are thus distinctive in accessing the structural variations of PDMS upon cross-linking.

DOI: 10.1021/acsami.5b00190
ACS Appl. Mater. Interfaces 2015, 7, 8515−8524

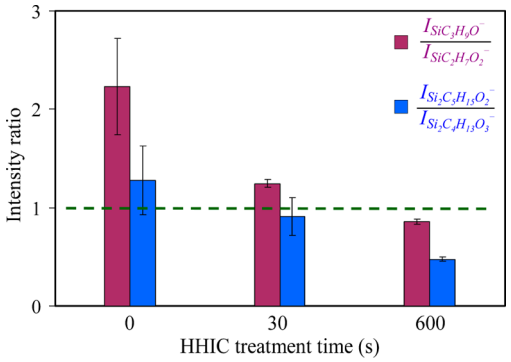

Figure 8. Intensity ratios of $SiC_3H_9O^-$ to $SiC_2H_7O_2^-$ and $Si_2C_5H_{15}O_2^-$ to $Si_2C_4H_{13}O_3^-$ The broken line shows the intensity ratio being equal to 1.

To make sense of the TOF-SIMS results shown in Figures 4 and 5, we tried an uncured PDMS (Sigma DMPS2x, viscosity 20 cSt). We spread this chemical (liquid) on a polypropylene film and conducted a TOF-SIMS experiment. The negative ion spectra showing the four species of $SiC_3H_9O^-$, $SiC_2H_7O_2^-$, $Si_2C_5H_{15}O_2^-$ and $Si_2C_4H_{13}O_3^-$ are shown in Figure 9. It is clear

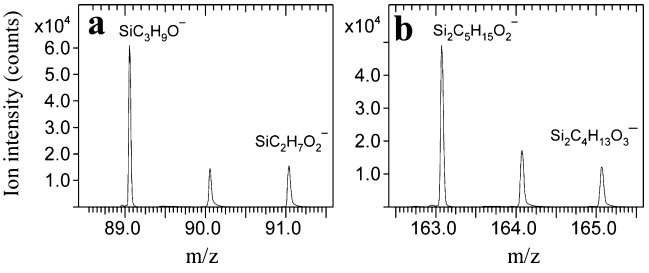

Figure 9. Negative secondary ion mass spectra in m/z ranges of (a) 88–92 (a) and (b) 162–165, obtained from a linear, uncured PDMS spread on a polypropylene film.

that the end-group containing species ($SiC_3H_9O^-$ and $Si_2C_5H_{15}O_2^-$) are much more abundant than the two species without the end-group ($SiC_2H_7O_2^-$ and $Si_2C_4H_{13}O_3^-$). The ratios of $SiC_3H_9O^-$ to $SiC_2H_7O_2^-$ and $Si_2C_5H_{15}O_2^-$ to $Si_2C_4H_{13}O_3^-$ are rather large, reaching 7.27 ± 0.20 and 7.46 ± 0.37, respectively. These experimental results are expected because an uncured PDMS would have much more end-groups. Our TOF-SIMS analyses thus hint that the cross-linking sites in the PDMS subjected to the HHIC treatment are perhaps preferentially associated with the end group of $Si(CH_3)_3$.

3.4. Mechanical Properties and Thickness of Cross-Linked PDMS Layer. The nanoindentation approach was used to measure the mechanical properties of the cross-linked layer for the HHIC-treated PDMS samples. The partial unloading method of the Hysitron system was used to probe the mechanical properties as a function of depth. The hardness and reduced modulus as a function of depth are shown in Figure 10. The hardness and modulus estimated on the very surface of the 180 min cured PDMS subjected to 5-s HHIC treatment are 0.084 and 0.57 GPa, respectively. They decreased rapidly with increased probe depth around 100 nm and then slowly reached a balance of 0.002 and 0.001 GPa, respectively. The decrement of PDMS surface modulus could be easily attributed to substrate effect, as discussed in a previous work involving a hard thin film on a soft substrate.[60,61] The variations of these mechanical properties as a function of depth indicated that the thickness of the cross-linked layer was less than 100 nm, as shown in Figure 10; and we need to establish another method for measure the cross-linking depth.

Shown in Figure 11a,b are topographic and phase shift images (1 × 1 μm), respectively, obtained on a cross section of the control (a 180 min cured PDMS sample). Figure 8e shows two profiles denoted as *a* and *b*, each isolated from the broken lines in the topographic and the phase shift images. The edge of the cross-sectioned PDMS was located using the CCD camera in the AFM system, followed by scanning large area AFM image. The surface of the cross section (cut by a razor blade) is relatively smooth, with a root-mean-square (RMS) roughness <3 nm. There is no phase shift contrast on the cross section of the control PDMS sample. The dark contrast in the phase shift image is due to the abrupt edge.

The AFM topographic and phase shift images obtained on cross section of the 600 s HHIC-treated PDMS are shown in Figure 11c,d. The profiles (denoted as *c* and *d*) isolated from the broken lines in those two images are shown in Figure 11f. The phase shift image clearly shows a higher contrast at the edge of the cross section, revealing that there is a layer more rigid[47] than the bulk of the PDMS. This layer ought to be the cross-linked PDMS resulted from the HHIC treatment.

Work has been done to measure the thickness of the cross-linked layer at the scale of less than one hundred nanometers.[11,62] Calculating the thickness of the cross-linked layer from the phase shift image is one of the methods since the phase shift angle depends on the surface viscoelasticity.[63] Taking the transition between the substrate and the cross-linked layer into consideration, the width of the bright contrast estimated from 80% of the peak height (Figure 11d,f) may be used to represent

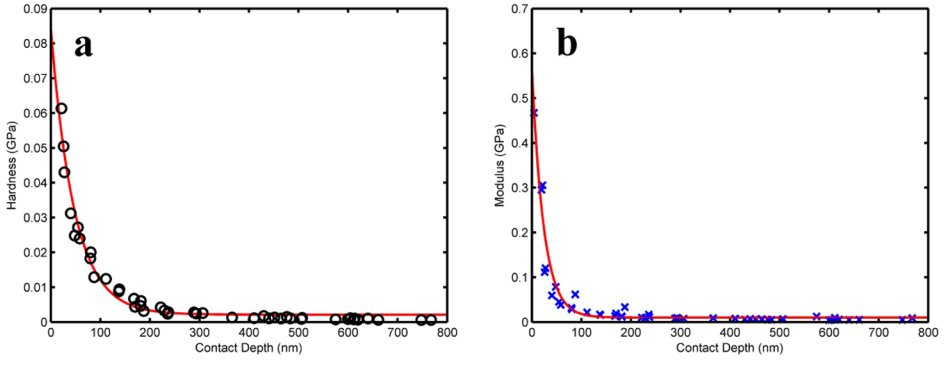

Figure 10. Hardness (a) and reduced modulus (b) as a function of depth probed on the HHIC-treated sample.

DOI: 10.1021/acsami.5b00190
ACS Appl. Mater. Interfaces 2015, 7, 8515–8524

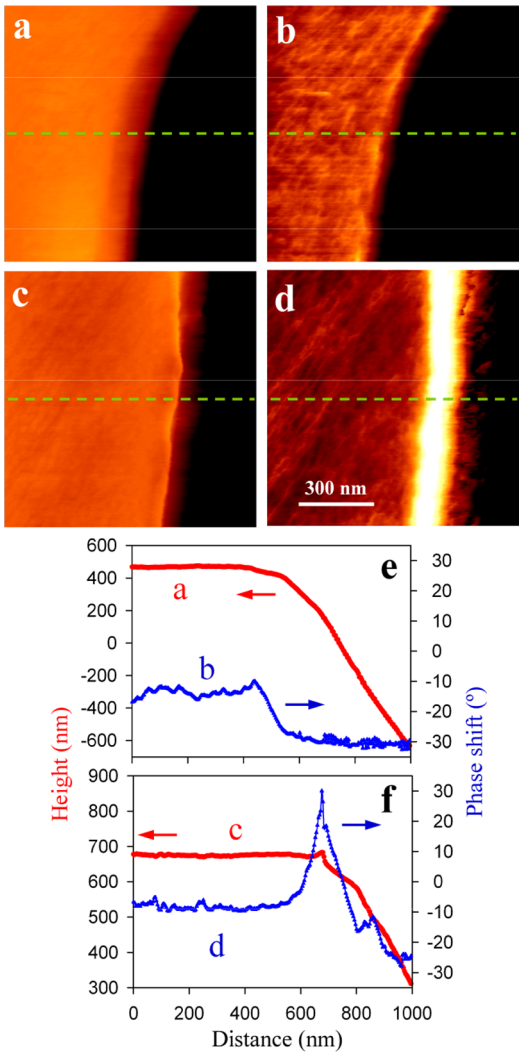

Figure 11. Topographic and phase images for the 180 min cured PDMS before (a, b) and after (c, d) the HHIC treatment for 600 s. The profiles isolated at the broken lines in panels a and b are shown in panel e, whereas those in panels c and d are shown in panel f.

the thickness of the layer. The width of the bright contrast thus estimated form the phase shift image in Figure 11d is 128 ± 12 nm for the 600 s HHIC-treated PDMS.

We also examined the surface morphology of the control, 30 s- and 600 s-treated PDMS samples. Shown in Figure 12 are topographic images obtained in an area of 1 × 1 μm on the three samples. There is no difference in morphology between the control and the 30 s-treated PDMS. For the 600 s-treated PDMS, there is a slight change in morphology. However, there are no significant changes in surface roughness, as all of the three samples show an RMS roughness of approximately 0.4 nm.

3.5. PDMS Characteristic Investigated by ATR-FTIR. We conducted ATR-FTIR analyses on the control and the HHIC-treated PDMS samples for 5, 10, 30, 60, 300 and 600 s for the purpose of checking whether there were significant changes in silicone functional groups upon the HHIC treatment. The FTIR spectra in wavenumber range 3800–600 cm^{-1} are shown in Figure 13a. The peaks at 1258, 1065, 1011 and 788 cm^{-1} are the fingerprint for silicone. As expected from the XPS results (Figure 3) showing that the oxidation occurred on the HHIC-treated PDMS was minimal, there was

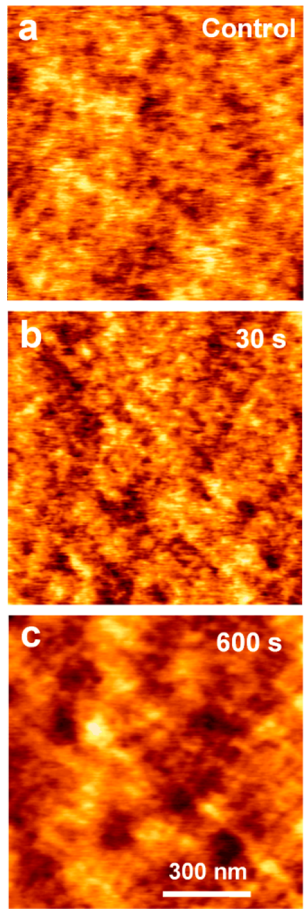

Figure 12. AFM images obtained on the control, the 30 s- and 600 s-treated PDMS samples. The height range for (a–c) is 4.3, 3.3 and 3.6 nm, respectively.

no OH groups detected from the ART-FTIR spectra, which would be a broad band covering the wavenumber range from 2800 to 3600 cm^{-1} as seen for PDMS subjected to UV/ozone treatment.[14,55]

The characteristic PDMS peaks and the CH_3 stretching mode peak are plotted in Figure 13b,c, respectively. As shown in Figure 13b, the two PDMS peaks at 1258 and 788 cm^{-1} are due to CH_3 deformation and CH_3 rocking in Si–CH_3, respectively, and the two adjacent peaks at 1065 and 1011 cm^{-1} are due to Si–O–Si asymmetric deformation.[42,54] Figure 13c shows the symmetric and asymmetric CH_3 stretching peaks at 2962 and 2906 cm^{-1}, respectively. As shown in the inset in Figure 13c are magnified peaks at 2962 cm^{-1} for all of the seven samples, there are slight reductions in intensities of these peaks for the HHIC-treated PDMS samples with increased treatment durations. Our ATR-FTIR results confirmed that the PDMS functionality as defined by the silicone functional groups were not alerted to the extent allowing a significant changes in the ART-FTR spectra for the HHIC-treated PDMS samples. By contrast, UV/ozone treatment readily change the chemistry of PDMS so that the peaks related to the methyl groups decreased significantly.[14,55]

4. CONCLUSIONS

We demonstrate for the first time that the HHIC technology is able to cross-link a controllable thickness of a cured PDMS substrate, resulting in enhanced mechanical properties but

DOI: 10.1021/acsami.5b00190
ACS Appl. Mater. Interfaces 2015, 7, 8515–8524

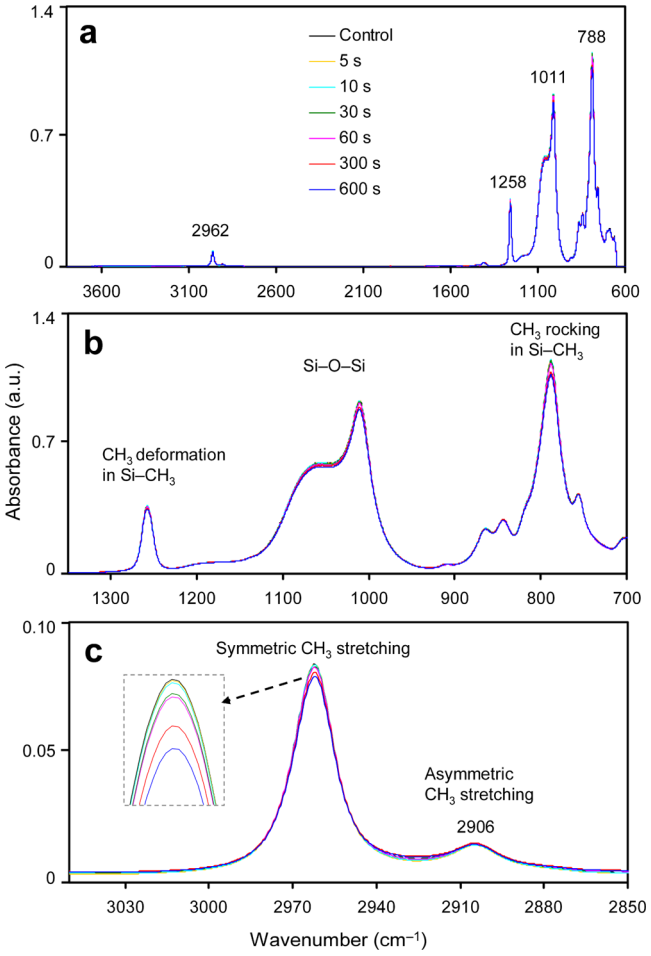

Figure 13. FTIR-ATR spectra in the wavenumber range of (a) 3800−600 cm^{-1}, (b) 1350−700 cm^{-1} and (c) 3050−2850 cm^{-1} obtained on the control and HHIC-treated PDMS samples for a serious of time as indicated in panel a.

without losing the inherent hydrophobicity as determined by contact angle measurements. This observation has been confirmed by XPS analyses, revealing that only minimal oxidation occurred on the PDMS surface upon the HHIC treatment. Both TOF-SIMS and nanoindentation studies confirm the surface cross-linking of PDMS upon HHIC treatment. The TOF-SIMS investigation further suggests that the preferential cross-linking sites are the end-groups of $Si(CH_3)_3$ and that the degree of cross-linking may be gauged by the intensity ratio between the end-group containing $SiC_3H_9O^-$ and a specific ion species of $SiC_2H_7O_2^-$ terminated by a hydroxyl at one end and an unpaired oxygen at the other. While, AFM phase imaging on its cross section confirms that the thickness of the cross-linked portion is on an order of 120 nm upon for HHIC-treated PDMS substrate for 600 s. Our work not only builds a solid fundamental study for applying PDMS through effectively tuning its cross-linked layer thickness by a new surface technique, HHIC but also establishes a well-posed calibration procedure for probing cross-linking systems.

AUTHOR INFORMATION

Corresponding Authors

*Y.L. E-mail: yu.liu@vip.163.com.

*H.-Y.N. E-mail: hnie@uwo.ca.

Author Contributions

⊗These authors contributed equally to this work.

Notes

The authors declare no competing financial interest.

ACKNOWLEDGMENTS

We thank Dr. Pal-Jen Wei from Hysitron Inc. for helping us on the nanoindentation experiment. Dr. Mark Biesinger of Surface Science Western is acknowledged for his assistance in the XPS experiment. Y.L. gratefully acknowledges the support from National Natural Science Foundation of China (Grant No. 51475484). C.Y.T thanks CAEP fund under 2013B0302058. Y.Z acknowledges the financial support from National Natural Science Foundation of China under 21104028.

REFERENCES

(1) Özçan, E. A.; Spontak, R. J.; Genzer, J. Towards the Development of a Versatile Functionalized Silicone Coating. *ACS Appl. Mater. Interfaces* **2014**, *6*, 22544−22552.

(2) Wang, Z.; Volinsky, A. A.; Gallant, N. D. Crosslinking Effect on Polydimethylsiloxane Elastic Modulus Measured by Custom-Built Compression Instrument. *J. Appl. Polym. Sci.* **2014**, *131*, 41050−1−4.

(3) Brown, X. Q.; Ookawa, K.; Wong, J. Y. Evaluation of Polydimethylsiloxane Scaffolds with Physiologically-Relevant Elastic Moduli: Interplay of Substrate Mechanics and Surface Chemistry Effects on Vascular Smooth Muscle Cell Response. *Biomaterials* **2005**, *26*, 3123−3129.

(4) Valamehr, B.; Jonas, S. J.; Polleux, J.; Qiao, R.; Guo, S.; Gschweng, E. H.; Stiles, B.; Kam, K.; Luo, T. M.; Witte, O. N.; Liu, X.; Dunn, B.; Wu, H. Hydrophobic Surfaces for Enhanced Differentiation of Embryonic Stem Cell-derived Embryoid Bodies. *Proc. Natl. Acad. Sci. U. S. A.* **2008**, *105*, 14459−14464.

(5) Kurpinski, K.; Chu, J.; Hashi, C.; Li, S. Anisotropic Mechanosensing by Mesenchymal Stem Cells. *Proc. Natl. Acad. Sci. U. S. A.* **2006**, *103*, 16095−16100.

(6) Guilak, F.; Cohen, D. M.; Estes, B. T.; Gimble, J. M.; Liedtke, W.; Chen, C. S. Control of Stem Cell Fate by Physical Interactions with the Extracellular Matrix. *Cell Stem Cell* **2009**, *5*, 17−26.

(7) Eroshenko, N.; Ramachandran, R.; Yadavalli, V. K.; Rao, R. R. Effect of Substrate Stiffness on Early Human Embryonic Stem Cell Differentiation. *J. Biol. Eng.* **2013**, *7*, 7−1−8.

(8) Gray, D. S.; Tien, J.; Chen, C. S. Repositioning of Cells by Mechanotaxis on Surfaces with Micropatterned Young's Modulus. *J. Biomed. Mater. Res., Part A* **2003**, *66*, 605−614.

(9) Engler, A.; Bacakova, L.; Newman, C.; Hategan, A.; Griffin, M.; Discher, D. Substrate Compliance versus Ligand Density in Cell on Gel Responses. *Biophys. J.* **2004**, *86*, 617−628.

(10) Rome, C.; Hueston, T. Silicone in the Oil and Gas Industry; Dow Corning Corp.: Midland, MI, 2002.

(11) Béfahy, S.; Lipnik, P.; Pardoen, T.; Nascimento, C.; Patris, B.; Bertrand, P.; Yunus, S. Thickness and Elastic Modulus of Plasma Treated PDMS Silica-like Surface Layer. *Langmuir* **2010**, *26*, 3372−3375.

(12) Qin, D.; Xia, Y.; Whitesides, G. M. Soft Lithography for Micro- and Nanoscale Patterning. *Nat. Protoc.* **2010**, *5*, 491−502.

(13) Luo, S. D.; Liu, T. Graphite Nanoplatelet Enabled Embeddable Fiber Sensor for in Situ Curing Monitoring and Structural Health Monitoring of Polymeric Composites. *ACS Appl. Mater. Interfaces* **2014**, *6*, 9314−9320.

(14) Berdichevsky, Y.; Khandurina, J.; Guttman, A.; Lo, Y.-H. UV/Ozone Modification of Poly(dimethylsiloxane) Microfluidic Channels. *Sens. Actuators, B* **2004**, *97*, 402−408.

(15) Odom, T. W.; Love, J. C.; Wolfe, D. B.; Paul, K. E.; Whitesides, G. M. Improved Pattern Transfer in Soft Lithography using Composite Stamps. *Langmuir* **2002**, *18*, 5314−5320.

(16) Delamarche, B. E.; Schmid, H.; Michel, B. Stability of Molded Polydimethylsiloxane Microstructures. *Adv. Mater.* **1997**, *9*, 741−746.

DOI: 10.1021/acsami.5b00190
ACS Appl. Mater. Interfaces 2015, 7, 8515−8524

(17) Schmid, H.; Michel, B. Siloxane Polymers for High-Resolution, High-Accuracy Soft Lithography. *Macromolecules* **2000**, *33*, 3042−3049.
(18) Hillborg, H.; Ankner, J. F.; Gedde, U. W.; Smith, G. D.; Yasuda, H. K.; Wikstro, K. Crosslinked Polydimethylsiloxane Exposed to Oxygen Plasma Studied by Neutron Reflectometry and Other Surface Specific Techniques. *Polymer* **2000**, *41*, 6851−6863.
(19) Ferguson, G. S.; Chaudhury, M. K.; Biebuyck, H. A.; George, M. W. Monolayers on Disordered Substrates: Self-Assembly of Alkyltrichlorosilanes on Surface-Modified Polyethylene and Poly (dimethylsiloxane). *Macromolecules* **1999**, *26*, 5870−5875.
(20) Yabu, H.; Saito, Y.; Nakamichi, Y.; Hirai, Y.; Fujinami, S.; Nakajima, K.; Nishi, T.; Shimomura, M. Self-Assembled Porous Templates Allow Pattern Transfer to Poly(dimethyl siloxane) Sheets Through Surface Wrinkling. *Polym. J. (Tokyo, Jpn.)* **2012**, *44*, 573−578.
(21) Trau, M.; Yao, N.; Kim, E.; Xia, Y.; Whitesides, G. M. Microscopic Patterning of Orientated Mesoscopic Silica through Guided Growth. *Nature* **1997**, *390*, 674−676.
(22) Chan, E. P.; Crosby, A. J. Fabricating Microlens Arrays by Surface Wrinkling. *Adv. Mater.* **2006**, *18*, 3238−3242.
(23) Chandra, D.; Yang, S.; Lin, P.-C. Strain Responsive Concave and Convex Microlens Arrays. *Appl. Phys. Lett.* **2007**, *91*, 251912.
(24) Huang, H.; Chung, J. Y.; Nolte, A. J.; Stafford, C. M. Characterizing Polymer Brushes via Surface Wrinkling. *Chem. Mater.* **2007**, *19*, 6555−6560.
(25) Thanawala, S. K.; Chaudhury, M. K. Surface Modification of Silicone Elastomer Using Perfluorinated Ether. *Langmuir* **2000**, *16*, 1256−1260.
(26) Aish, E. H.; Crocker, M.; Ladipo, F. T. Tripodal Titanium Silsesquioxane Complexes Immobilized in Polydimethylsiloxane (PDMS) Membrane: Selective Catalysts for Epoxidation of Cyclohexene and 1-Octene with Aqueous Hydrogen Peroxide. *J. Catal.* **2010**, *273*, 66−72.
(27) Guedes, D. F. C.; Mac Leod, T. C. O.; Gotardo, M. C. A. F.; Schiavon, M. A.; Yoshida, I. V. P.; Ciuffi, K. J.; Assis, M. D. Investigation of a New Oxidative Catalytic System Involving Jacobsen's Catalyst in the Absence of Organic Solvents. *Appl. Catal., A* **2005**, *296*, 120−127.
(28) Parton, R. F.; Vankelecom, I. F. J.; Tas, D.; Janssen, K.; Knops-Gerrits, P.-P.; Jacobs, P. A. Membrane Occluded Catalysts: A Higher Order Mimic with Improved Performance. *J. Mol. Catal. A: Chem.* **1996**, *113*, 283−292.
(29) Mac Leod, T. C. O.; Barros, V. P.; Faria, A. L.; Schiavon, M. A.; Yoshida, I. V. P.; Queiroz, M. E. C.; Assis, M. D. Jacobsen Catalyst as a P450 Biomimetic Model for the Oxidation of an Antiepileptic Drug. *J. Mol. Catal. A: Chem.* **2007**, *273*, 259−264.
(30) Mac Leod, T. C. O.; Kirillova, M. V.; Pombeiro, A. J. L.; Schiavon, M. A.; Assis, M. D. Mild Oxidation of Alkanes and Toluene by Tert-Butylhydroperoxide Catalyzed by an Homogeneous and Immobilized Mn(salen) Complex. *Appl. Catal., A* **2010**, *372*, 191−198.
(31) Man, C.; Jiang, P.; Wong, K.; Zhao, Y.; Tang, C.; Fan, M.; Lau, W.; Mei, J.; Li, S.; Liu, H.; Hui, D. Enhanced Wetting Properties of a Polypropylene Separator for a Lithium-Ion Battery by Hyperthermal Hydrogen Induced Cross-Linking of Poly(ethylene oxide). *J. Mater. Chem. A* **2014**, *2*, 11980−11986.
(32) Wang, X.; Zhang, T.; Kobe, B.; Lau, W. M.; Yang, J. Grafting of Polyelectrolytes onto Hydrocarbon Surfaces by High-Energy Hydrogen Induced Cross-Linking for Making Metallized Polymer Films. *Chem. Commun.* **2013**, *49*, 4658−4660.
(33) Thompson, D. B.; Trebicky, T.; Crewdson, P.; McEachran, M. J.; Stojcevic, G.; Arsenault, G.; Lau, W. M.; Gillies, E. R. Functional Polymer Laminates from Hyperthermal Hydrogen Induced. *Langmuir* **2013**, *27*, 14820−14827.
(34) Karamdoust, S.; Yu, B.; Bonduelle, C. V.; Liu, Y.; Davidson, G.; Stojcevic, G.; Yang, J.; Lau, W. M.; Gillies, E. R.; Chem, J. M. Preparation of Antibacterial Surfaces by Hyperthermal Hydrogen Induced Cross-Linking of Polymer Thin Films. *J. Mater. Chem.* **2012**, *22*, 4881−4889.
(35) Bonduelle, C. V.; Lau, W. M.; Gillies, E. R. Preparation of Protein- and Cell-Resistant Surfaces by Hyperthermal Hydrogen Induced Cross-Linking of Poly(ethylene oxide). *ACS Appl. Mater. Interfaces* **2011**, *3*, 1740−1748.
(36) Liu, Y.; Yang, D. Q.; Nie, H.-Y.; Lau, W. M.; Yang, J. Study of a Hydrogen-Bombardment Process for Molecular Cross-Linking within Thin Films. *J. Chem. Phys.* **2011**, *134*, 074704.
(37) Good, R. J. Contact Angle, Wetting, and Adhesion: A Critical Review. *J. Adhes. Sci. Technol.* **1992**, *6*, 1269−1302.
(38) Hollander, J. M.; Jolly, W. L. X-ray Photoelectron Spectroscopy. *Acc. Chem. Res.* **1970**, *3*, 193−199.
(39) Hillborg, H.; Gedde, U. W. Hydrophobicity Recovery of Polydimethylsiloxane after Exposure to Corona Discharges. *Polymer* **1998**, *39*, 1991−1998.
(40) Orhan, J.-B.; Parashar, V. K.; Flueckiger, F.; Gijs, M. A. M. Internal Modification of Poly(dimethylsiloxane) Microchannels with a Borosilicate Glass Coating. *Langmuir* **2008**, *24*, 9154−9161.
(41) Efimenko, K.; Wallace, W. E.; Genzer, J. Surface Modification of Sylgard-184 Poly(dimethyl siloxane) Networks by Ultraviolet and Ultraviolet/Ozone Treatment. *J. Colloid Interface Sci.* **2002**, *254*, 306−315.
(42) Maji, D.; Lahiri, S. K.; Das, S. Study of Hydrophilicity and Stability of Chemically Modified PDMS Surface using Piranha and KOH Solution. *Surf. Interface Anal.* **2012**, *44*, 62−69.
(43) Benninghoven, A. Chemical Analysis of Inorganic and Organic Surfaces and Thin Films by Static Time-of-Flight Secondary Ion Mass Spectrometry (TOF-SIMS). *Angew. Chem., Int. Ed. Engl.* **1994**, *33*, 1023−1043.
(44) Nie, H.-Y. Revealing Different Bonding Modes of Self-Assembled Octadecylphosphonic Acid Monolayers on Oxides by Time-of-Flight Secondary Ion Mass Spectrometry: Silicon vs Aluminum. *Anal. Chem.* **2010**, *82*, 3371−3376.
(45) Muramoto, S.; Brison, J.; Castner, D. G. Exploring the Surface Sensitivity of TOF-Secondary Ion Mass Spectrometry by Measuring the Implantation and Sampling Depths of Bin and C60 Ions in Organic Films. *Anal. Chem.* **2012**, *84*, 365−372.
(46) Martínez, N. F.; García, R. Measuring Phase Shifts and Energy Dissipation with Amplitude Modulation Atomic Force Microscopy. *Nanotechnology* **2006**, *17*, S167−S172.
(47) Nie, H.-Y.; Taylor, A. R.; Lau, W. M.; MacFabe, D. F. Subcellular Features Revealed on Unfixed Rat Brain Sections by Phase Imaging. *Analyst* **2011**, *136*, 2270−2276.
(48) Oliver, W. C.; Pharr, G. M. Measurement of Hardness and Elastic Modulus by Instrumented Indentation: Advances in Understanding and Refinements to Methodology. *J. Mater. Res.* **2011**, *19*, 3−20.
(49) Zheng, Z.; Xu, X.; Fan, X.; Lau, W. M.; Kwok, R. W. M.; Wai, R.; Kwok, M. Ultrathin Polymer Film Formation by Collision-Induced Cross-Linking of Adsorbed Organic Molecules with Hyperthermal Protons. *J. Am. Chem. Soc.* **2004**, *126*, 12336−12342.
(50) Lau, W. M.; Zheng, Z.; Wang, Y. H.; Luo, Y.; Xi, L.; Wong, K. W.; Wong, K. Y. Cross-Linking Organic Semiconducting Molecules by Preferential C-H Cleavage via "Chemistry with a Tiny Hammer". *Can. J. Chem.* **2007**, *85*, 859−865.
(51) Zheng, Z.; Wong, K. W.; Lau, W. C.; Wai, R.; Kwok, M.; Lau, W. M. Unusual Kinematics-Driven Chemistry: Cleaving C À H but Not COO À H Bonds with Hyperthermal Protons To Synthesize Tailor-Made Molecular. *Chem.—Eur. J.* **2007**, *13*, 3187−3192.
(52) Zheng, Z.; Kwok, M.; Ming, W. A New Cross-Linking Route via the Unusual Collision Kinematics of Hyperthermal Protons in Unsaturated Hydrocarbons: the Case of Poly(trans-isoprene). *Chem. Commun.* **2006**, 3122−3124.
(53) Egitto, F. D.; Matienzo, L. J. Transformation of Poly(dimethylsiloxane) into Thin Aurface Dilms of SiO_x by UV/Ozone Treatment. Part I: Factors Affecting Modification. *J. Mater. Sci.* **2006**, *41*, 6362−6373.
(54) Bodas, D.; Khan-Malek, C. Formation of More Stable Hydrophilic Surfaces of PDMS by Plasma and Chemical Treatments. *Microeletronic Eng.* **2006**, *83*, 1277−1279.

DOI: 10.1021/acsami.5b00190
ACS Appl. Mater. Interfaces 2015, 7, 8515−8524

(55) Lai, C. L.; Fu, Y. J.; Chen, J. T.; An, Q. F.; Liao, K. S.; Fang, S. C.; Hu, C. C.; Lee, K. R. Pervaporation Separation of Ethanol/Water Mixture by UV/O_3-Modified PDMS Membranes. *Separation Purification Technol.* **2012**, *100*, 15−21.
(56) Oláh, A.; Hillborg, H.; Vancso, G. J. Hydrophobic Recovery of UV/Ozone Treated Poly(dimethylsiloxane): Adhesion Studies by Contact Mechanics and Mechanism of Surface Modification. *Appl. Surf. Sci.* **2005**, *239*, 410−423.
(57) Bancroft, G. M.; Nesbitt, H. W.; Ho, R.; Shaw, D. M.; Tse, J. S.; Biesinger, M. C. Toward a Comprehensive Understanding of Solid-State Core-Level XPS Linewidths: Experimental and Theoretical Studies on the Si 2p and O 1s Linewidths in Silicates. *Phys. Rev. B* **2009**, *80*, 075405(1−13).
(58) Louette, P.; Bodino, F.; Pireaux, J.-J. Poly(dimethyl siloxane) (PDMS) XPS Reference Core Level and Energy Loss Spectra. *Surf. Sci. Spectra* **2005**, *12*, 38−43.
(59) Lee, D. H.; Yang, S. Surface Modification of PDMS by Atmospheric-Pressure Plasma-Enhanced Chemical Vapor Deposition and Analysis of Long-Lasting Surface Hydrophilicity. *Sens. Actuators, B* **2012**, *162*, 525−434.
(60) Yoo, Y.-H.; Lee, W.; Shin, H. Spherical Nano-indentation of a Hard Thin Film/Soft Substrate Layered System: I. Critical Indentation Depth. *Modell. Simul. Mater. Sci. Eng.* **2004**, *12*, 59−67.
(61) Vlachos, D. E.; Markopoulos, Y. P.; Kostopoulos, V. 3-D Modeling of Nanoindentation Experiment on a Coating-Substrate System. *Comput. Mech.* **2001**, *27*, 138−144.
(62) Mills, K.; Zhu, X. The Mechanical Properties of a Surface-Modified Layer on Polydimethylsiloxane. *J. Mater. Res.* **2008**, *23*, 37−48.
(63) Magonov, S. N.; Elings, V.; Whangbo, M. Phase Imaging and Stiffness in Tapping-Mode Atomic Force Microscopy. *Surf. Sci.* **1997**, *375*, L385−L391.

DOI: 10.1021/acsami.5b00190
ACS Appl. Mater. Interfaces 2015, 7, 8515−8524